10. Left-lateral and normal aftershocks on planes subparallel to the mainshock could conceivably occur where the fault slipped but only if there was complete dynamic overshoot (a complete reversal of shear stress on the fault plane as a result of the mainshock slip). This behavior is extremely unlikely. Theoretical rupture calculations indicate that dynamic overshoot is a small effect, with a value at most of ~15% of the difference between the static and dynamic friction levels [for example, R. Burridge and G. S. Halliday, *Geophys. J. R. Astron. Soc.* **25**, 261 (1971)]. For dynamic overshoot to explain left-lateral and normal aftershocks in the regions of right-lateral and reverse stress drop certain conditions would be required. The dynamic frictional strength of the fault would have to be nearly zero, and the overshoot would have to be so extreme as to change completely the sign of stress on the fault and cause failure in the opposite direction in the aftershock.
11. G. C. Beroza, *Bull. Seismol. Soc. Am.* 81, 1603 (1991).
12. J. H. Steidl, R. J. Archuleta, S. H. Hartzell, *ibid.*, p. 1573.
13. D. J. Wald, D. V. Helmberger, T. H. Heaton, *ibid.*, p. 1540.
14. There is an inherent nonuniqueness in the inference of fault slip from seismic observations because the problem is underdetermined. Regularization techniques give solutions subject to a priori constraints such as smoothness. See A. H. Olson and J. G. Anderson, *Geophys. J.* **94**, 443 (1988).
15. We calculated ΔT using the rupture model (*7*) in a general program [L. Ericksen, thesis, Stanford University (1986)] for calculating stresses in an elastic half space due to rectangular dislocation sources. We have approximated the spatially varying slip model with 8554 dislocations.
16. H. Kanamori and K. Satake, *Geophys. Res. Lett.* **17**, 1179 (1990).
17. There is an ambiguity when one discriminates the aftershock fault plane from the auxiliary plane. However, because of the symmetry of the stress tensor and moment tensors, the projection of the mainshock-induced traction onto the slip vector is the same for both possible fault planes. This quantity may be calculated from the stress change ΔT and the aftershock moment tensor **M**. The normalized
$$\mathbf{M} = 1/2(\mathbf{ns} + \mathbf{sn})$$
and
$$1/2\mathbf{M}:\Delta\mathbf{T} = \mathbf{s}\cdot\Delta\mathbf{T}\cdot\mathbf{n} = \mathbf{n}\cdot\Delta\mathbf{T}\cdot\mathbf{s}$$
but these last two expressions are simply the projection of the slip vectors onto the mainshock traction change. This quantity has been used to study variations in the stress field after the 1987 Whittier Narrows earthquake [A. J. Michael, *J. Geophys. Res.* **96**, 6303 (1991)]. We define a spatially variable stress change (stress drop) to determine the sign of ΔT using displacements and traction changes determined from the elastostatic solution. If the stress decreased, then $\Delta T\cdot u < 0$ and, if the stress increased, then $\Delta T\cdot u > 0$. Left-lateral and normal aftershocks for which $\Delta T < 0$ and $\mathbf{M}:\Delta T > 0$ would imply that there was complete dynamic overshoot.
18. The inner product of two vectors, in this case traction and slip vectors, will be positive 50% of the time if their orientation is random.
19. Because slip in the Loma Prieta mainshock was a combination of right-lateral and reverse on a dipping plane, it is incapable of explaining the unexpected left-lateral and normal mechanisms on subparallel planes. Moreover, no slip model can explain incompatible pairs of events in the same area, especially regions far from the mainshock. That is, an earthquake cannot cause stress to change in two directions at once. If slip occurred over a larger area than in the model (*7*), even more left-lateral and normal aftershocks would have occurred in regions of stress drop and would require that there was complete dynamic overshoot. If slip occurred over a smaller area than in the model, the aftershocks that occurred far from the hypocenter are even more difficult to understand.
20. M. D. Zoback and G. C. Beroza, *Geology*, in press.
21. The extremely low strength of the San Andreas fault is indicated by the absence of a frictionally generated heat-flow anomaly [J. N. Brune, T. L. Henyey, R. Roy, *J. Geophys. Res.* **74**, 3821 (1969); see also A. H. Lachenbruch, *ibid.* **85**, 6097 (1980)]. Observations in central California also show that the direction of maximum principal stress is nearly perpendicular to the San Andreas fault, so that there is little resolved shear stress on it [M. D. Zoback *et al.*, *Science* **238**, 1105 (1987); V. S. Mount and J. Suppe, *Geology* **15**, 1143 (1987)].
22. J. W. Gephart and D. W. Forsyth, *J. Geophys. Res.* **89**, 9305 (1984). We find that the quantity $(S_1 - S_3)/(S_2 - S_3) = 0.7$, which indicates that the intermediate and minimum principal stresses, S_2 and S_3, are comparable.
23. The average residual of ~11° and the generally small residuals over the entire aftershock zone indicate that a predominantly uniform stress tensor of near fault-normal compression is consistent with the observed aftershock diversity.
24. R. H. Sibson, in (*9*).
25. A. Nur and J. R. Booker, *Science* **175**, 885 (1972); A. H. Lachenbruch, in (*21*).
26. Aftershocks of the 1984 Morgan Hill (magnitude = 6.1) earthquake were analyzed with a similar technique [D. H. Oppenheimer, P. A. Reasenberg, R. W. Simpson, *J. Geophys. Res.* **93**, 9007 (1988)]. Unlike the Loma Prieta earthquake, the Morgan Hill event had aftershocks that occurred on the mainshock fault plane had the same right-lateral mechanism as the mainshock. However, the off-fault seismicity did show evidence of fault-normal compression and was cited as evidence that the Calaveras fault is weak.
27. We thank D. Oppenheimer for his fault-plane solutions and B. Ellsworth, A. Michael, P. Segall, and R. Simpson for helpful discussions. Supported by a National Science Foundation Presidential Young Investigator Award (G.B.), a Shell Faculty Career Initiation Grant (G.B.), and U.S. Geological Survey grant 14-08-0001-G1853 (M.Z.).

17 March 1992; accepted 15 October 1992

Domain Structures in Langmuir-Blodgett Films Investigated by Atomic Force Microscopy

L. F. Chi, M. Anders, H. Fuchs,* R. R. Johnston, H. Ringsdorf

Investigations of phase-separated Langmuir-Blodgett films by atomic force microscopy reveal that on a scale of 30 to 200 micrometers, these images resemble those observed by fluorescence microscopy. Fine structures (less than 1 micrometer) within the stearic acid domains were observed, which cannot be seen by conventional optical microscopic techniques. By applying the force modulation technique, it was found that the elastic properties of the domains in the liquid condensed phase and grains observed within the liquid expanded phase were comparable. Small soft residues in the domains could also be detected. The influence of trace amounts of a fluorescence dye on the micromorphology of monolayers could be detected on transferred films.

Langmuir-Blodgett (LB) and related thin organic films have been the objects of increasing technological and scientific interest over the past 20 years (*1–4*). Optimization of the macroscopic physical properties of these systems requires a detailed understanding of their structure-property relations on a microscopic scale, including the structure of transferred LB films on solid substrates, the nucleation of crystalline phases, and their phase transitions. At the air-water interface the phase states of lipid monolayers and their transitions, such as the formation of domains in the coexistence region of liquid condensed–liquid expanded (LC-LE) phases, have been investigated by fluorescence microscopy (*5–9*). Similar studies on transferred LB films at the air-substrate interface, however, have rarely been reported (*10*). Fluorescence microscopy is limited to structures larger than 1 μm in diameter. Electron microscopy has also been applied to image domain structures (*11, 12*). However, the imaging technique applied (phase contrast transmission

L. F. Chi, M. Anders, H. Fuchs, BASF AG, Polymer Research Laboratory, ZKM/T-J543, W-6700 Ludwigshafen, Germany.
R. R. Johnston and H. Ringsdorf, Institute of Organic Chemistry, Johannes Gutenberg University, J. J. Becherweg 18-20, W-6500 Mainz, Germany.
*To whom correspondence should be addressed.

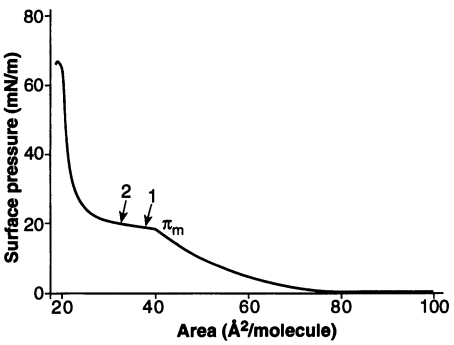

Fig. 1. Isotherm of surface pressure (π) versus area per molecule of stearic acid on a poly(ethyleneimine) (PEI, M_n = 1800)–containing aqueous subphase. The conditions are as follows: T = 20°C, V_c = 2.84 Å² molecule^{-1} min^{-1}. The pressure of the main phase transition (π_m, position 1) and different positions for film transfers are marked with arrows.

electron microscopy and scanning transmission electron microscopy) did not resolve submicrometer features in real space within the domains. Therefore, it remained difficult to investigate the early stages of domain formation in coexisting phases. In addition, little is known about the dynamics of these systems in the submicrometer regime after transfer onto solid substrates under ambient conditions.

With the advent of the atomic force microscope (AFM) (*13*), it became clear that the surface morphology and the defect structures of LB films could be investigated on the molecular scale in real space, as demonstrated by several groups (*14–19*). Recently, the local tribological behavior of mixed LB films studied by lateral force microscopy (LFM) was reported (*20*). However, little has been done to address the submicrometer morphological changes related to phase transitions in phase-separated LB films. Because AFM can be used to image surface areas from the molecular scale up to tenths of millimeters in size, it should represent an ideal tool for macroscopic and microscopic studies on these systems.

Here we report AFM studies on the micromorphology of domains in the LC phase. As a model system, stearic acid (C_{18}) LB films were deposited on poly(ethyleneimine) (PEI) layers on a mica substrate. This acid forms LC domains (3 to 5 μm in diameter) on a PEI-containing aqueous subphase at room temperature. These domains looked homogeneous in the fluorescence microscope (*21*). We used the same system to prepare the films for our AFM experiments (*22*). The monolayers were prepared on a commercial double trough (KSV Chemical Corporation) in a clean room under class 10 conditions. Mica was used as a substrate. The polymeric counterions of PEI_{1800} in the aqueous subphase form thin layers on the mica substrate during the preparation of the film, which strongly adhere to the mica surface (*10*). The monolayer was compressed at a controlled rate (V_c) up to the main transition pressure (π_m, see the pressure-area isotherm in Fig. 1). The pressure was then held constant during the film deposition. The transfer ratio was greater than unity, because the area per molecule decreased spontaneously in the plateau region. This determined the transfer position in the isotherm. The deposition speed (V_d) was well controlled. To study the influence of fluorescence dyes on the micromorphology of the domains of transferred films, separate C_{18} monolayers were prepared in the presence of 0.25 mol% sulforhodamine lipid (DPPE-SR), frequently used as a dye in fluorescence microscopy experiments.

We carried out AFM imaging in the repulsive mode in air with a commercial system (Park Scientific Instruments). The experiments were done in the same clean room as the LB experiments. Two different scanners were used for surface inspection: a 250-μm scanner and a 10-μm scanner (*23*). Soft cantilevers 200 μm long with an integrated pyramidal tip, exhibiting a nominal spring constant of 0.032 N m^{-1}, were used for all the measurements.

To obtain information on the local modulus of elasticity, we applied force spectroscopy using phase-sensitive detection as described by Maivald *et al.* (*24*). We used a cantilever that was softer by five orders of magnitude than that used by Maivald *et al.* A small modulation amplitude (dz = 0.6 Å) is mandatory in our case, because the total film thickness is only about 25 Å.

By scanning the film surface up to 200 by 200 μm^2, we were able to observe the domains transferred onto the substrate (the depositions near the center of the plateau region, position 2 in Fig. 1). Images measuring 30 by 30 μm^2 are shown in Fig. 2, A and B. The average domain size and its shape vary as a function of the monolayer compression rate (Fig. 2A: V_c = 2.84 $Å^2$ $molecule^{-1}$ min^{-1}; Fig. 2B: V_c = 8.52 $Å^2$ $molecule^{-1}$ min^{-1}; in both cases, V_d = 4 mm min^{-1}). Faster

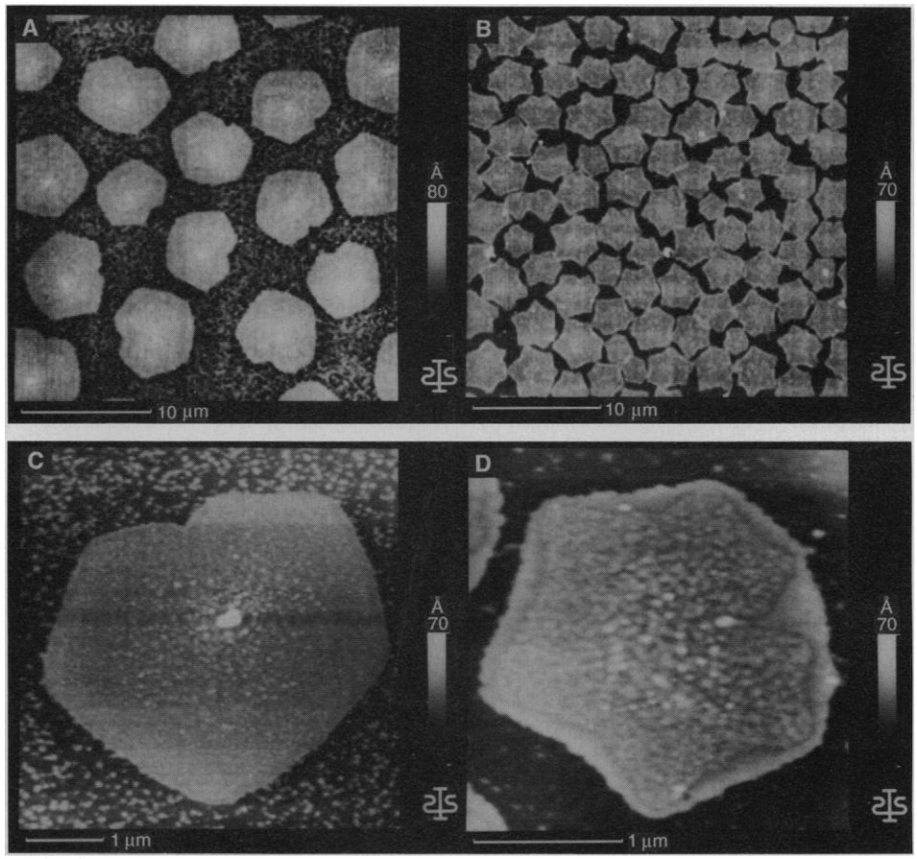

Fig. 2. AFM images of pure stearic acid films deposited on a PEI-coated mica surface. All films were transferred at position 2 in Fig. 1. The samples were prepared under the following conditions: V_c = 2.84 $Å^2$ $molecule^{-1}$ min^{-1} and V_d = 4 mm min^{-1} for (**A**) and (**C**), V_c = 8.52 $Å^2$ $molecule^{-1}$ min^{-1} and V_d = 4 mm min^{-1} for (**B**) and (**D**). Faster compression of the monolayer leads to smaller domains with a less uniform shape.

Fig. 3. Topographical image (left) and the corresponding map of the local stiffness (right) of a single domain. High brightness in the right part of the figure corresponds to a high value of the modulus of elasticity.

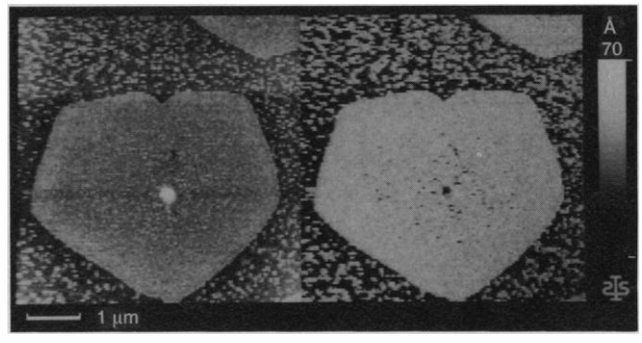

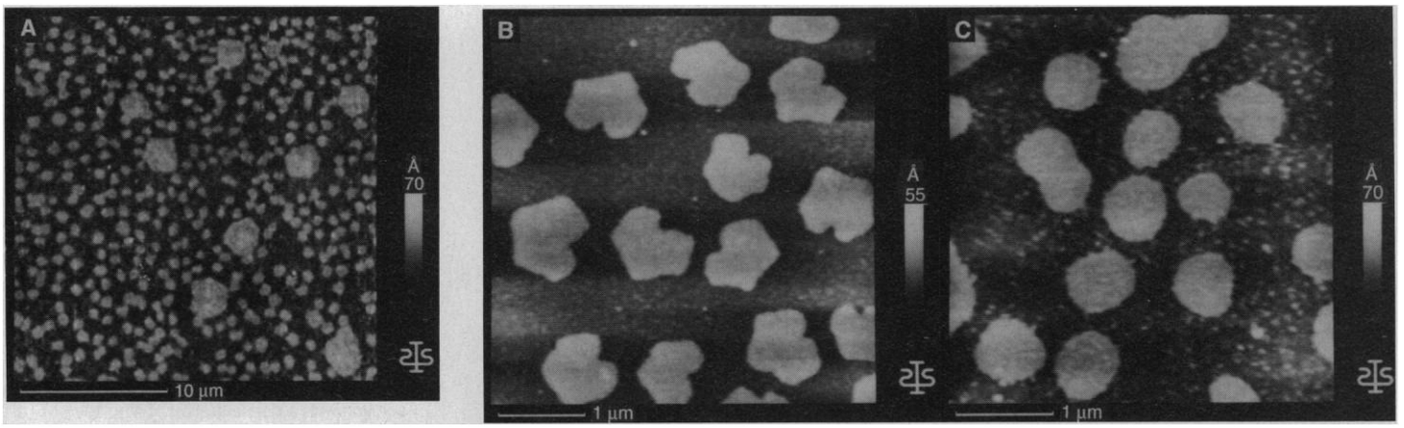

Fig. 4. AFM images of pure stearic acid transferred at the onset of the main phase-transition region (position 1 in Fig. 1): V_c = 2.84 Å^2 molecule^{-1} min^{-1} and V_d = 4 mm min^{-1}. Image (**B**) was taken within 1 hour after film deposition [image (**A**)], and image (**C**) was taken 4 days later on the same sample. The domains changed from a polygonal to a circular shape several hours after film deposition.

compression of the monolayer leads to smaller domains with a less uniform shape. These results agree with the results of fluorescence microscopy experiments, thus confirming the capability of the AFM to image the domain structures nondestructively.

The height difference between the LC phase and the LE phase in our systems is about 15 to 20 Å as measured with the AFM. This indicates that the AFM tip, which responds to the viscoelastic properties of a sample, penetrates partially into the LE phase, giving rise to the high contrast observed. This is consistent with a difference in packing density between LC and LE phases of about 30% (*12*). Nevertheless, the imaging is not destructive. Small grains within the LE phase (Fig. 2C) do not change their shape or position during repeated imaging.

By increasing the magnification beyond the resolution limit of the optical microscope, we can observe the fine structures within a single domain (Fig. 2, C and D): Near the center of the domains bright spots often show up; the roughness of the domain edges differs from that of the center parts; grains 0.03 to 0.05 μm in diameter were detected and became more pronounced because of aging. This indicates a dynamic behavior even of the transferred film at the air-substrate interface. Another interesting observation is that the micromorphology of single domains depends strongly on the compression speed. A high compression speed leads to domains composed of several subdomains with their boundaries visible (Fig. 2D). The edges of these domains show a texture different from that of the main part of the domains. These internal boundaries and the pronounced edge areas are not seen in Fig. 2C, indicating relatively homogeneous packing caused by the lower compression rate during the domain formation. Outside the domains, in the liquid-like region of the coexistence phase, we observed numerous grains that resemble in size the grains inside the LC domains (0.02 to 0.07 μm in diameter). These grains may serve as nuclei for LC domain formation.

The topographic image (Fig. 3, left) and the modulus of elasticity (Fig. 3, right) were simultaneously recorded. High brightness in the right part of the figure corresponds to a high value of the modulus of elasticity. The modulus of the grains in the LE phase is as high as the modulus of the grains in the crystalline phase. For the protrusions (bright spots in the left part of the figure) found in the LC domains the modulus is as low as that

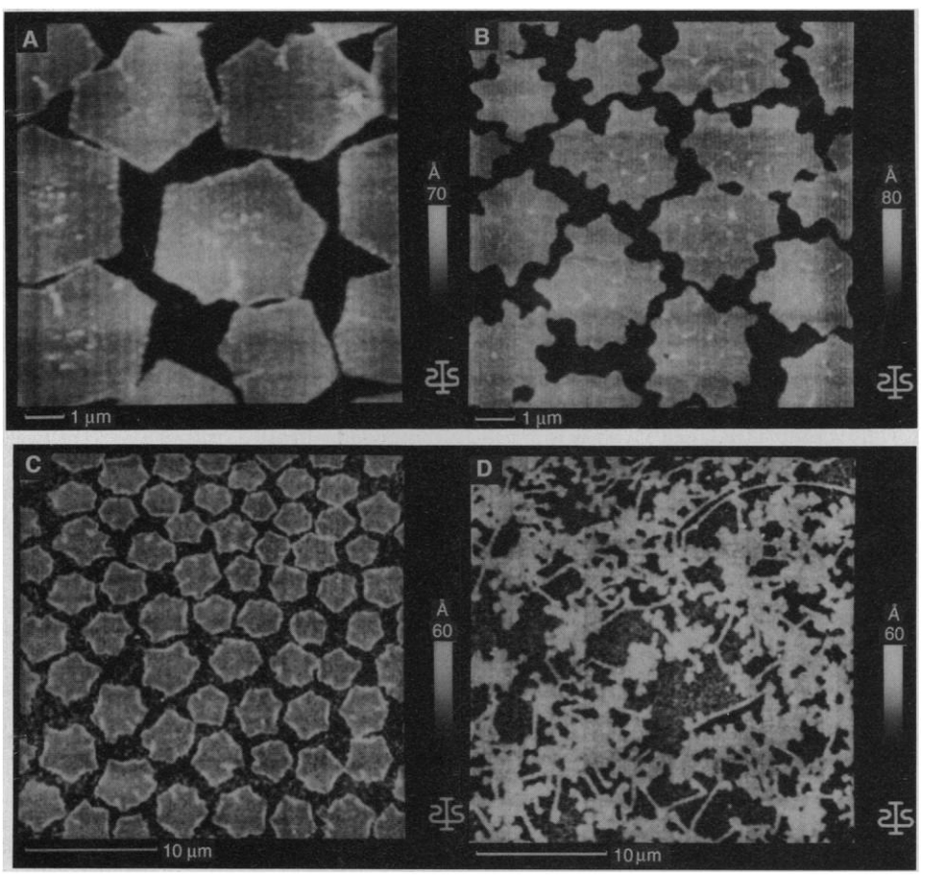

Fig. 5. AFM images of stearic acid films without (**A**) and with (**B** through **D**) fluorescence dye (0.25 mol% DPPE-SR). All the films were transferred at position 2 in Fig. 1. V_c = 5.68 Å^2 molecule^{-1} min^{-1} and V_d = 20 mm min^{-1} for (A) and (B); V_c = 8.52 Å^2 molecule^{-1} min^{-1} and V_d = 50 mm min^{-1} for (**C**) and V_c = 2.84 Å^2 molecule^{-1} min^{-1} and V_d = 4 mm min^{-1} for (D) (the same as for the sample without fluorescence dye, as shown in Fig. 2, A and C). The presence of the fluorescence dye clearly influences the domain structures on transferred films.

in the LE phase (except for the grains). This suggests that these protrusions should be regarded as noncrystalline residues. The modulus of elasticity in the protrusions was about 10^8 Pa (that is, one order higher than that of rubber), whereas the modulus in the LC domains was substantially higher.

Monolayers transferred at the onset of the main phase-transition region (position 1 in Fig. 1; all other conditions are the same as for Fig. 2, A and C) exhibited a few bigger domains (>2 μm in diameter) surrounded by many smaller domains (~0.5 μm in diameter, Fig. 4A). In the case of a freshly prepared sample imaged within 1 hour after deposition, the shape of these small domains is similar to that of the large domains (compare Fig. 4B and Fig. 2A). However, the domains change their shape spontaneously on the solid substrates (Fig. 4C) within several hours during storage (humidity, 42 ± 1%; temperature, 21° ± 0.5°C). This phenomenon can thus only be detected by applying the AFM technique within a short time after film deposition. It is likely that, in the case of a high compression speed, the small domains consolidated and merged into the LC domains with visible boundaries as shown in Fig. 2D; in the case of a low compression speed, the domains grow at the expense of smaller ones, leading to better packed LC domains, as shown in Fig. 2C.

In fluorescence microscopy studies it is necessary that trace amounts of fluorescence dyes be added to the system under investigation. The influence of the dye molecules on the phase behavior of the monolayers is generally thought to be negligible in low concentrations (<3 mol%). With the AFM we were able to investigate the potential influence of dye molecules in even very low concentrations (here 0.25 mol%) as an impurity on the domain structures on transferred films. Figure 5, A and B, shows domain structures without and with fluorescence dye, respectively [all other conditions were kept exactly the same (V_c = 5.68 Å^2 molecule^{-1} min^{-1} and V_d = 20 mm min^{-1})]. Obviously, the presence of the fluorescence dye does affect the domain structures. In addition, the domains of the dye-containing systems change their shapes drastically from "star-like" (Fig. 5C) to "fiber-like" (Fig. 5D) during the film deposition, and the changes are very sensitive to the transfer conditions (in Fig. 5C, V_c = 8.52 Å^2 molecule^{-1} min^{-1} and V_d = 50 mm min^{-1}; in Fig. 5D, V_c = 2.84 Å^2 molecule^{-1} min^{-1} and V_d = 4 mm min^{-1}). These results indicate that care must be taken in extrapolating the results obtained from dye-labeled monolayers at the air-water interface to the transferred films.

REFERENCES AND NOTES

1. H. Kuhn, D. Möbius, H. Bücher, in *Physical Methods of Chemistry*, A. Weissberger and B. Rossiter, Eds. (Wiley, New York, 1972), vol. 1 (part 3b), p. 650.
2. G. G. Roberts, *Langmuir-Blodgett Films* (Plenum, New York, 1990).
3. A. Ulman, *An Introduction to Ultrathin Organic Films: From Langmuir-Blodgett to Self-Assembly* (Academic Press, Boston, 1991).
4. H. Fuchs, H. Ohst, W. Prass, *Adv. Mater.* **3**, 10 (1991).
5. V. von Tscharner and H. M. McConnell, *Biophys. J.* **36**, 409 (1981).
6. M. Lösche, E. Sackmann, H. Möhwald, *Ber. Bunsenges. Phys. Chem.* **87**, 848 (1983).
7. P. Meller, R. Peters, H. Ringsdorf, *Colloid Polym. Sci.* **267**, 97 (1989).
8. H. Möhwald, *Thin Solid Films* **159**, 1 (1988).
9. C. M. Knobler, *Science* **249**, 870 (1990).
10. L. F. Chi, R. R. Johnston, N. Kimizuka, T. Kunitake, H. Ringsdorf, *Langmuir* **8**, 1360 (1992).
11. A. Fischer and E. Sackmann, *Nature* **313**, 299 (1985).
12. ———, *J. Colloid Interface Sci.* **112**, 1 (1986).
13. G. Binnig, C. F. Quate, Ch. Gerber, *Phys. Rev. Lett.* **56**, 930 (1986).
14. O. Marti *et al.*, *Science* **239**, 50 (1988).
15. E. Meyer *et al.*, *Nature* **349**, 398 (1991).
16. H. G. Hansma *et al.*, *Langmuir* **7**, 1051 (1991).
17. J. Garnaes, D. K. Schwartz, R. Viswanathan, J. A. N. Zasadzinski, *Nature* **357**, 54 (1992).
18. H. Fuchs, L. F. Chi, L. M. Eng, K. Graf, *Thin Solid Films* **210–211**, 655 (1992).
19. L. F. Chi, L. M. Eng, K. Graf, H. Fuchs, *Langmuir* **8**, 2255 (1992).
20. R. M. Overney *et al.*, *Nature* **359**, 133 (1992).
21. L. F. Chi, R. R. Johnston, H. Ringsdorf, *Langmuir* **7**, 2323 (1991).
22. We dissolved stearic acid (Fluka) in chloroform (HPLC quality, Baker) to get a spreading solution with a concentration of 5 × 10^{-3} M. Branched poly(ethyleneimine) with an average molecular weight of M_n = 1800 (Polysciences) was dissolved in deionized water (water resistance, 19 megohms; Christ System), providing an aqueous solution with a concentration of 4 × 10^{-3} M.
23. The 250-μm scanner allows inspections from 0.25 mm to the submicrometer scale, thus providing a wide overlap with the resolution of a light microscope. The 10-μm scanner allows imaging down to the molecular scale.
24. P. Maivald *et al.*, *Nanotechnology* **2**, 103 (1991).

25. We thank M. Lösche for stimulating discussions.

8 July 1992; accepted 21 October 1992

An Inhibitor of p34^{CDC28} Protein Kinase Activity from *Saccharomyces cerevisiae*

Michael D. Mendenhall

The p34^{CDC28} protein from *Saccharomyces cerevisiae* is a homolog of the p34^{cdc2} protein kinase, a fundamental regulator of cell division in all eukaryotic cells. Once activated it initiates the visible events of mitosis (chromosome condensation, nuclear envelope breakdown, and spindle formation). The p34^{CDC28} protein also has a critical role in the initiation of DNA synthesis. The protein kinase activity is regulated by cycles of phosphorylation and dephosphorylation and by periodic association with cyclins. An endogenous 40-kilodalton protein (p40) originally identified as a substrate of the p34^{CDC28} protein kinase was purified. The p40 protein bound tightly to p34^{CDC28} and inhibited the activity of the kinase. The p40 protein may provide another mechanism to regulate p34^{CDC28} protein kinase activity.

The p34$^{CDC28/cdc2}$ protein kinase (p34) is a universal regulator of mitosis in eukaryotes (*1*). Its activity is required for entry into the DNA replicative phase (S phase) and for the initiation of mitosis (M phase) (*2*). Deactivation of p34 is required for exit from mitosis (*3*). The regulation of p34 protein kinase activity, subcellular localization, and substrate interaction is complex. Three primary modes of control have been described: (i) activation resulting from association with particular members of a family of cyclins (*4*), the synthesis and stability of which are tightly controlled (*5*); (ii) activating and deactivating cycles of phosphorylation and dephosphorylation at multiple sites on the p34 polypeptide (*6*); and (iii) controlled synthesis of p34 itself (*7*). Here, evidence is presented for another regulatory mechanism—the binding of an inhibitory protein.

Lucille P. Markey Cancer Center and Department of Biochemistry, University of Kentucky, Lexington, KY 40536.

The protein kinase activity of p34, which is encoded by the *CDC28* gene of the budding yeast *Saccharomyces cerevisiae*, was originally demonstrated in immunoprecipitates from crude cell extracts (*8*). In these experiments, a 40-kD substrate (p40) coimmunoprecipitated with p34. Phosphorylation of p40 by p34 was cell cycle–dependent (*9*). Protein extracts taken from cells arrested in S phase or M phase had active p34 protein kinase (*10*), but phosphorylation of p40 was not detected in p34 immunoprecipitates (*9*). Extracts from cells arrested in the prereplicative phase (G_1) by mating pheromone treatment or nutrient deprivation had no detectable p34 protein kinase activity, but when these extracts were mixed with p34 immunoprecipitates from S or M phase–arrested cells, p40 phosphorylation was observed. These results suggested that p40 is only present in cells arrested in G_1 or is modified in S and M phase cells such that it cannot bind to, or be phosphorylated by, p34.